Springer

Acta Mechanica Sinica

CrossMark click for updates

• RESEARCH PAPER •

Acta Mech. Sin., Vol. 40, 723296 (2024)
https://doi.org/10.1007/s10409-023-23296-x

Geophysical fluid dynamics in the hypergravity field

Harry Yeh*

School of Civil & Construction Engineering, Oregon State University, Corvallis, OR 97331, USA

Received June 30, 2023; accepted August 8, 2023; published online September 15, 2023

Hypergravity can be realized by creating a field imposed by centripetal acceleration in a centrifuge apparatus. Such an apparatus is often used to test soil response in geotechnical engineering problems. Here we present the potential usage of a centrifuge apparatus to study various topics in hydrodynamics. The scaling law associated with hydrodynamics is first reviewed, and the advantage of controlling the body force is described. One of the perceived disadvantages in such experiments is the unwanted presence of the Coriolis effect in the centrifuge. However, we propose exploiting this effect to our advantage to study geophysical fluid-dynamic problems that occur particularly in the equatorial region.

Hypergravity, Scaling, Geophysical fluid dynamics, Centrifuge

Citation: H. Yeh, Geophysical fluid dynamics in the hypergravity field, Acta Mech. Sin. 40, 723296 (2024), https://doi.org/10.1007/s10409-023-23296-x

1. Introduction

The term hypergravity is used to describe the condition when the body force exceeds that by gravity. Controlling the body force can be achieved by use of a centrifuge apparatus. In the area of geotechnical engineering, the field-scale conditions are often simulated in the small-scale physical model in the centrifuge for a variety of geotechnical problems, such as slope stability, consolidation, liquefaction, and soil-structure interaction. This is because hypergravity created by the centrifuge can scale up soil stresses in a small model to mimic the field condition. To produce the same soil stresses in the small-scale model, the weight of the model specimen must be increased by the same ratio in the length scale of the field condition. Creating the identical soil-stress condition in the model is crucial for geotechnical testing because a soil's constitutive relation (relation between stresses and strains) is neither linear nor isotropic, hence without imposing hypergravity, it is difficult to interpret the results from the model for the corresponding soil response in the field.

Figure 1 exhibits a typical centrifuge facility, which was specifically designed and constructed for geotechnical engineering testing. This is a large apparatus of its kind, having an arm length of 9.1 m, and through the action of spinning, is capable of creating a body force up to 75 times that of gravity ($75g$) with a payload capacity of 4500 kg. The apparatus can accommodate a model container of 2.1 m long, 1.0 m wide and 0.75 m high in the bucket (see Fig. 1 (b)). Suppose we use a soil specimen that is 1.8 m long, 0.7 m wide, and 0.6 m deep placed in the container, then this model would represent the 135 m long, 52 m wide, and 45 m deep soil in the field under the centripetal acceleration of $75g$. Evidently, the use of a centrifuge gives us an advantage by creating realistic soil stresses in the small model. On the other hand, the small-size model together with the enhanced time-lapse rate by hypergravity causes difficulties in instrumentation; sensor probes must be very small in size and must be capable of acquiring the data at a very high sampling rate with high resolution. In fact, the recent advances in instrumentation technologies have made centrifuge use practical.

Previously, there have been several centrifuge studies that involve fluid flows. Sassa and Sekiguchi [1] examined soil response under water-wave actions. Exton et al. [2-4] modeled tsunami-like runup and drawdown flow processes over sandy sediments. Harry et al. [5] explored the boulder pick-up mechanism under the surging flow motion. Several

*Corresponding author. E-mail address: harry@oregonstate.edu (Harry Yeh)
Executive Editor: Chao Sun

engineering works are also reported as demonstrations of coastal structure performance [6-8]. All of those are, however, related to geotechnical problems.

Here we explore the use of the centrifuge to investigate a variety of problems in hydrodynamics. As stated, hypergravity experiments performed in a centrifuge can provide the same body-force field in the model as the corresponding large-scale field condition. This is an advantage over model studies which do not control the body force. It is noted that the model must be small in size because of the space available in the centrifuge bucket (see Fig. 1). Therefore, instruments implemented in the model must be small and durable under the large body force. One of the side effects is caused by the fact that the model specimen is in rotational motion with the finite arm length. This causes the Coriolis effects. This is an unwanted side effect for the centrifuge experiments. Here, we instead explore the hypergravity experiments to utilize this induced Coriolis effect: in particular, to study problems in geophysical fluid dynamics in which the Coriolis effect is important. This is the primary theme of this paper.

In the following sections, the scaling law for hypergravity experiments for fluid flows in general is systematically introduced. This is accomplished by non-dimensionalizing the governing equations and boundary conditions. Performing a simple experiment of the surge flow from the sluice gate, the effects of hypergravity are demonstrated. We point out that hypergravity experiments can be advantageous for studying bubble (and also droplet) dynamics and density currents. Utilization of the unavoidable Coriolis effect in the centrifuge experiments is discussed, and we propose hypergravity experiments in geophysical fluid dynamics, especially for phenomena in the equatorial region.

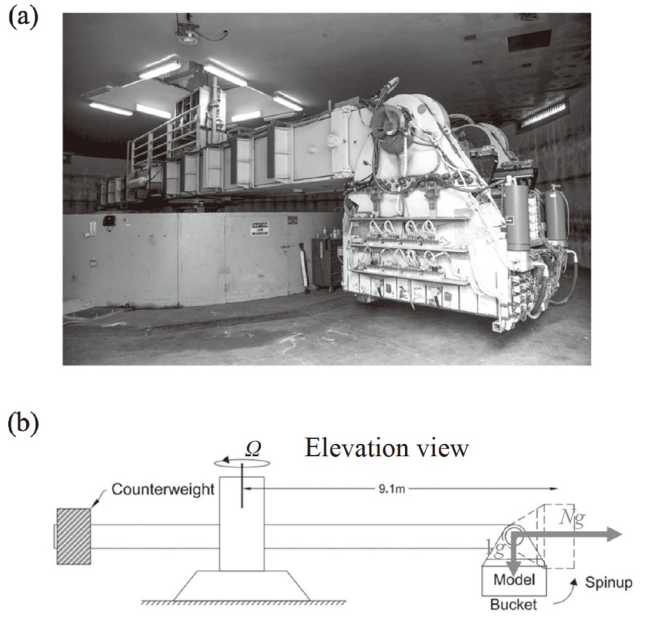

Figure 1 (a) A photo of the 9.1-m radius geotechnical centrifuge apparatus at the University of California, Davis; (b) a schematic drawing. When the beam rotates, the bucket swings up on its hinge so that the pseudo-force from the centripetal acceleration becomes normal to the model.

For convenience, from hereinafter, we use the term "prototype" to present actual physical field conditions, while the term "model" is the scaled-down representation of the corresponding prototype. Flow problems considered here are limited to those with the assumption of incompressible fluids.

2. Scaling law for hypergravity models

The scaling law for geotechnical hypergravity models is aimed at realizing identical fluid pressures and vertical soil stresses present in the prototype. This can be achieved by applying the body force increased by the geometric ratio of the prototype to the model: in other words, scaling the body force by $g_r = 1/L_r$, where the subscript r represents the scale factor (viz. $g_r = g_m/g_p$ and $L_r = L_m/L_p$: the subscripts m and p denote, respectively, the quantities of model and prototype). This is the basis of geotechnical hypergravity experiments.

It is however important to recognize that the scaling $g_r = 1/L_r$ is not a requirement for the model in hydrodynamics. In fact, for usual laboratory studies in fluid dynamics, the body force cannot be controlled; hence $g_r = 1$. Unlike the soil media, the continuum hypothesis is accepted for fluids unless the molecular-level motions are considered (e.g., rarefied gas flows). Thus, the mechanics of fluids are based on the well-established constitutive relation based on the Newtonian hypothesis.

The governing equation for fluid motions is the Navier-Stokes equation that represents the conservation of linear momentum, and can be written in the following form for incompressible fluids in the rotating reference frame:

$$\rho(\partial\mathbf{u}/\partial t + \mathbf{u}\cdot\nabla\mathbf{u} + 2\boldsymbol{\Omega}\times\mathbf{u}) = -\nabla p + \nabla\cdot(\mu\nabla\mathbf{u}) + \rho\mathbf{G}, \quad (1)$$

where $\mathbf{u}$ is the fluid velocity, $\boldsymbol{\Omega}$ is the constant angular velocity of the rotating frame and $\Omega = |\boldsymbol{\Omega}|$, $\mathbf{G} = \mathbf{g} + \Omega^2\mathbf{r}$ is the body force per unit mass—combination of gravitational and centrifugal forces imposed in the hypergravity experiments, $\mathbf{r}$ is the radial vector from the axis of the rotating reference frame, ρ is the fluid density, p is the pressure, and μ is the viscosity. Nondimensionalizing Eq. (1) yields

$$S_t\partial\mathbf{u}_*/\partial t_* + \mathbf{u}_*\cdot\nabla_*\mathbf{u}_* + R_b^{-1}\boldsymbol{\Omega}_*\times\mathbf{u}_* = -E_u\nabla_* p_* + R_e^{-1}\nabla_*^2\mathbf{u}_* + F_d^{-2}\mathbf{G}_*, \quad (2)$$

expressing the normalized variables with the subscript "$_*$". The non-dimensional numbers appeared in Eq. (2) are

Strouhal number: $S_t = L_0/u_0 t_0$,

Rossby number: $R_b = u_0/2\Omega L_0$,

Euler number: $E_u = p_0/\rho u_0^2$,

Reynolds number: $R_e = \rho u_0 L_0/\mu$,

Froude number: $F_d = u_0/\sqrt{GL_0}$,

in which $G = \left|\mathbf{g} + \Omega^2 \mathbf{r}_0\right|$ denotes the magnitude of the body force at the fixed position $\mathbf{r}_0$. Note that, when the distance from the axis of the rotating reference frame is much greater than the length scale of the flow, $L_0 \ll \left|\mathbf{r}_0\right|$, the magnitude of the normalized body force $\left|\mathbf{G}_*\right|$ is constant and unity. By choosing proper characteristic scales for (L_0, t_0, u_0, p_0) in the operation of nondimensionalization of Eq. (1), the order of magnitude of each term expressed with the subscript "$*$" in Eq. (2) can be made to have a magnitude on the order of unity. Consequently, the relative magnitudes of the forces involved in Eq. (1) are represented by the values of non-dimensional parameters $(S_t, R_b, E_u, R_e, F_d)$ in Eq. (2), and those parameters are independent. In other words, the magnitudes of the parameters represent which forces are dominant for a given situation and/or for a focus of the problem. This in turn yields a justification of the model by properly simplifying the problem by neglecting unimportant term(s).

To complete the formulation, we must consider the boundary conditions. On a stationary solid boundary in the reference frame, the no-slip condition is imposed, viz. $\mathbf{u}_* = 0$. At the fluid-fluid interface, the dynamic condition must be satisfied. In the nondimensionalized form:

$$\left[\!\left[\left\{ -E_u\, p_*\, \delta_{ij} + R_e^{-1}\left[\nabla_* \mathbf{u}_* + \left(\nabla_* \mathbf{u}_*\right)^{\mathrm{T}}\right]\right\} \cdot \mathbf{n} \right]\!\right] = -W_b^{-1}(\kappa_{1*} + \kappa_{2*})\,\mathbf{n}, \tag{3}$$

where δ_{ij} is the Kronecker delta, the superscript T denotes transpose, $\mathbf{n}$ is the unit vector normal to the interface, and $[\![\,\cdot\,]\!]$ represents the jump condition of the stress vector across the boundary, for example see Ref. [9]. The right-hand-side of Eq. (3) represents the surface tension effect, κ_{1*} and κ_{2*} are the principal curvatures of the interface. The non-dimensional parameter that emerges in the dynamic boundary condition at the fluid-fluid interface is

Weber number: $W_b = \rho_0 u_0^2 L_0/\gamma$,

where γ is the surface tension.

When all of the nondimensional parameters $(S_t, R_b, E_u, R_e, F_d, W_b)$ of the prototype match those of the model, then, the mathematical representation for the prototype and the corresponding model is identical. Consequently, the model and the prototype are dynamically equivalent, hence achieving the dynamic similitude.

All of the nondimensional parameters $(S_t, R_b, E_u, R_e, F_d, W_b)$ are, however, difficult to match simultaneously, because the fluid properties (e.g., ρ, μ, γ) and the body force G are difficult to control. As a result, the model needs to be compromised, and the deviation from the perfect similitudes is called the "scale effect", which induces uncertainty in a small-scale-model study to predict the corresponding large-scale prototype. Controlling the body force G by hypergravity provides us with a means to reduce the scale effect for the gravity-controlled flow problems in which Froude number matching is important: therefore $u_r = \sqrt{g_r L_r}$ is required, which is called the Froude law.

3. Froude-number matching

The models for gravity-driven flows, such as open-channel flows, water waves, and density currents, should satisfy the Froude law: namely, the Froude number of the prototype matches with that of the model. For the model under Earth's gravitational field ($g_r = 1$), it is unavoidable that the Reynolds number of the prototype mismatches that of the model, because it is impractical to use a fluid other than water in the model: the fluid density ρ and viscosity μ are difficult to control for the desirable values. To satisfy the Froude-number matching with the length-scale ratio L_r, the velocity scale must be $u_r = \sqrt{L_r}$ under the gravitational field. This condition results in a Reynolds-number value that is smaller than that of the prototype: that mismatches by $L_r^{3/2}$. After accepting this mismatch in the Reynolds number, a common tactic to minimize the scale effects is to use a large-scale model to achieve a large Reynolds number. As inferred from Eq. (2), the viscous effect becomes unimportant when the Reynolds number is "sufficiently" large. When the prototype flows are turbulent and the model flow is also completely turbulent, then, the scale effect by mismatching the Reynolds number is expected to be insignificant. Unfortunately, this requires a large-scale model, and it is unknown how large of a model is sufficient and what the resulting errors would be quantitative.

Under the hypergravity environment, the body force in the model can be enhanced to a desired value, say $g_m = Ng$ (or $g_r = N$) where g is the magnitude of Earth's gravitational acceleration. If we use the geometric similitude with L_r, then to maintain the Froude law, the velocity scale in the model should be $\sqrt{NL_r}$, and the time scale would be $\sqrt{L_r/N}$. Using the same fluid in the model as the prototype still leads to a discrepancy in the Reynolds number, but the ratio of Reynolds number of the model to that of the prototype would be $N^{1/2}L_r^{3/2}$. Clearly, the mismatch can be mitigated by the factor $N^{1/2}$ in the hypergravity experiments. In other words, the Reynolds number of the model can be enhanced by the order of magnitude when we impose $N = 100$, i.e., $g_m = 100g$, for example. This is significant in scale-effect

reduction, because this enhancement could be sufficient to make the model flow to be completely turbulent. Although formidable, further improvement could be achieved by using a less viscous liquid in the model. In fact, at least theoretically, both the Froude number and Reynolds number would match if we use a fluid with smaller viscosity: i.e., the kinematic viscosity μ/ρ of the model should be $\left(N^{1/2}L_r^{3/2}\right)^{-1}$ that of the prototype.

Using the centrifuge shown in Fig. 1, the effect of hypergravity was demonstrated by Exton et al. [3]. They conducted a pair of experiments with a $L_r = 1/40$ scaled-down model: one under Earth's gravity ($G = g$) and the other under hypergravity on the centrifuge ($G = 40g$ or $N = 40$). Water colored with blue dye is released from the reservoir on the surface of quiescent clear water in the tank by suddenly lifting the vertical sluice gate. The results are shown in Fig. 2. The flow depth of the leading flow is approximately 0.045 m in the 1-*g* model and 0.030 m in the 40-*g* model: the slight difference in flow depth is due to the boundary layer: note that the boundary-layer thickness is inversely proportional to the square root of flow speed. The speed of the leading tongue of the flow is 1.75 m/s for the 1-*g* model and 10.5 m/s for the 40-*g* model; hence, the flow speed in the 40-*g* centrifuge case is very close to the predicted value ($= 1.75\times40^{1/2} = 11.1$ m/s). The resulting Reynolds number R_e for the 1-*g* model is 8.2×10^4 and 3.2×10^5 for the 40-*g* model. The Froude number for the 1-*g* model is 2.6, which approximately matches that of the 40-*g* model ($F_r = 3.1$).

In Fig. 2, it is evident that the appearance of the flow is affected by hypergravity: the flow is very energetic, exhibiting break-up bubbles for the 40-*g* case. On the other hand, smooth and large irregular features of the water surface are present for the 1-*g* case. Note that the dyed water can be clearly seen in the surging flow for the 1-*g* case, while that is not obvious for the 40-*g* case because of the presence of numerous bubbles formed in the high Reynolds-number flow. The region ahead of the surge front represents the still clear water. For the 40-*g* case, the transparent water shows the tank bed. On the other hand, for the 1-*g* case, we detect several ripple ring formations, in spite of the fact that the surge front has not reached that portion. The examination of the video footage reveals that those ripples are caused by water drops landing on the water surface: the water drops are generated by a splashed-up effect during the opening motion of the sluice gate. Such drops are not present for the 40-*g* case, because the enhanced body force reduces the maximum elevation attained by the droplets.

The difference in appearance of bubbles and droplets shown in Fig. 2 must be due to the mismatch in the Weber number (i.e., surface tension effect). Under the Froude law, the mismatch in the Weber number is L_r^2 for the 1-*g* model, whereas the mismatch is NL_r^2 for the *N*-*g* model (or L_r if $N = 1/L_r$); hence the surface tension effect is much stronger in the 1-*g* model than that in the 40-*g* model. It is commented that the hypergravity environment is potentially beneficial to investigate bubble (and/or droplet) dynamics. For example, a relevant parameter to study bubble rise in a liquid is the Bond number: $B_o = \Delta\rho G L_0^2/\gamma$, in which $\Delta\rho$ is the difference in density of the two fluid phases. Under the hypergravity field, the Bond number can be matched by setting $N = L_r^{-2}$. For example, bubbles at a water depth of 4 m can be simulated in a water depth of 0.5 m in the centrifuge model by imposing $G = 64g$ ($N = 64$).

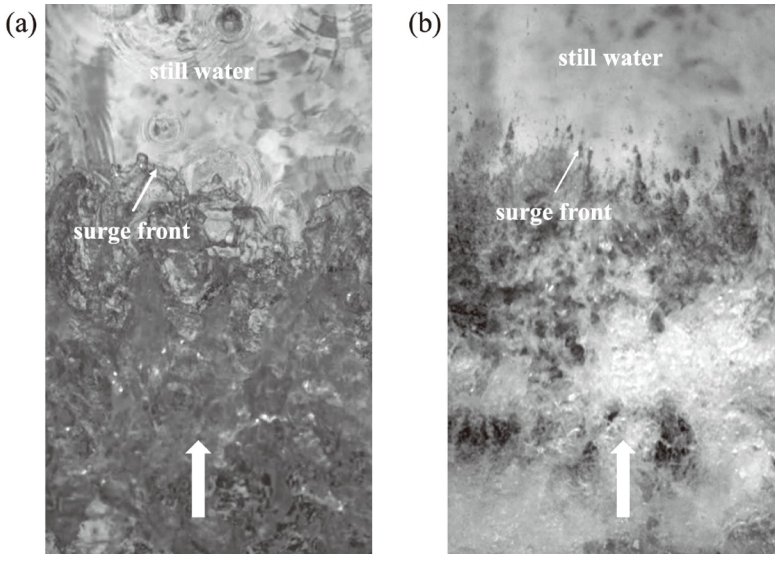

Figure 2 Top-down views of the surge front generated in the centrifuge apparatus: (a) under 1-*g* condition, and (b) under 40-*g* condition. Flow with dye is released on the clear still water from the sluice gate (from the bottom of the photos). The view shown is approximately 23 cm wide and 39 cm long.

Another potential benefit of the hypergravity experiments may be for the study of density currents and/or internal bores. For example, the density currents generated in a navigation lock are investigated by Lingel [10]. Conducting the field measurements at the Hiram M. Chittenden Locks in Seattle, Washington, the field data are compared with the scaled-down laboratory experiments. The mixing processes between the intruding brackish-water current and the ambient fresh water are quantified using two techniques: (1) the Thorpe scale Δ_T that gives a length scale for an overturning motion at the interface [11], and (2) the available potential energy of the fluctuation (APEF) that estimates the amount of potential energy in an overturn available for kinetic energy [12,13]. While the Thorpe scales measured in the field are consistent with those measured in the laboratory, the APEF values in the laboratory were found to be significantly larger than the values in the field. Lingel [10] conjectured that this is because the density fluctuations are greater in the laboratory than in the field. The gradient Richardson number of the mixed layer is typically lower in the laboratory than in the field either due to the fact that there was background turbulence with smaller energetic eddies in the field and/or that the mixing transition was not reached in the laboratory [14]. Hypergravity experiments may resolve such discrepancies between the field data and the laboratory experiments.

4. Geophysical fluid dynamics

When the centrifuge is used for hypergravity experiments, the third term on the left-hand side of Eq. (1) is present. This is the Coriolis effect, which is an important factor in geophysical fluid dynamics under the influence of Earth's rotation Ω: see Fig. 3(a). For the Reynolds number being large (hence, negligible viscous effect), Eq. (1) can be written as

$$\begin{aligned}
&\frac{\mathrm{D}u}{\mathrm{D}t} - fv + 2\Omega w\cos\varphi = -\frac{1}{\rho}\frac{\partial p}{\partial x},\\
&\frac{\mathrm{D}v}{\mathrm{D}t} + fu = -\frac{1}{\rho}\frac{\partial p}{\partial y},\\
&\frac{\mathrm{D}w}{\mathrm{D}t} - 2\Omega u\cos\varphi = -\frac{1}{\rho}\frac{\partial p}{\partial z} - g.
\end{aligned} \tag{4}$$

Here the velocity vector is presented by $\mathbf{u} = (u, v, w)$ and $\mathbf{x} = (x, y, z)$ = (east, north, up), $f = 2\Omega\sin\varphi$ is the Coriolis parameter, φ is the latitude, and D/Dt denotes the material derivative. A majority of the problems in geophysical fluid dynamics are analyzed under the "traditional approximation", which neglects the horizontal component of Earth's rotation. The justification is that the depth of oceans is thin compared to the radius of the Earth and the large-scale motions are nearly horizontal. Eliminating the horizontal component of rotation, $2\Omega\cos\varphi$, and further approximating the Coriolis effect by the Taylor series expansion, i.e., the β-plane approximation, the form of the "traditional approximation" of Eq. (4) can be written as

$$\begin{aligned}
&\frac{\mathrm{D}u}{\mathrm{D}t} - (f_0 + \beta y)v = -\frac{1}{\rho}\frac{\partial p}{\partial x},\\
&\frac{\mathrm{D}v}{\mathrm{D}t} + (f_0 + \beta y)u = -\frac{1}{\rho}\frac{\partial p}{\partial y},\\
&\frac{\mathrm{D}w}{\mathrm{D}t} = -\frac{1}{\rho}\frac{\partial p}{\partial z} - g,
\end{aligned} \tag{5}$$

where f_0 is the Coriolis parameter at the fixed latitude φ_0. Under the traditional approximation, it is common to perform the laboratory experiments with the use of a rotating table as illustrated in Fig. 3(b). It is noted that the condition created in the rotating table represents the polar region.

The foregoing condition of the "traditional approximation" cannot be realized in the centrifuge apparatus. Instead,

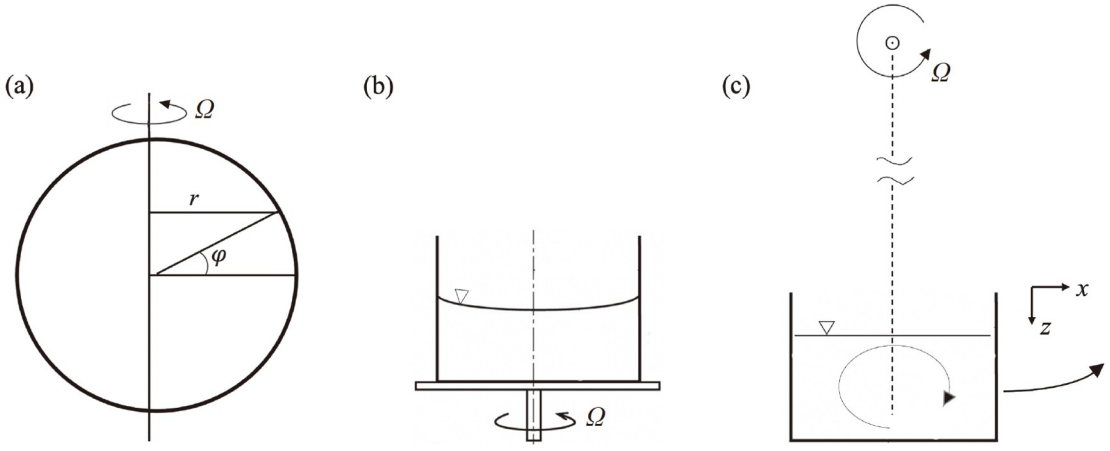

Figure 3 (a) Sketch of the Earth; φ is the latitude, Ω = 1 revolution/day, r is the radial distance from the rotation axis. (b) Rotating table apparatus typically used in the laboratory experiments for geophysical fluid dynamics. (c) Plan view of centrifuge apparatus for the hypergravity experiments: the model bucket rotates about o and x points in the azimuthal direction and z points in the radial direction; the Coriolis effect induces a circulation pattern in the x-z plane as shown.

the centrifuge at a high rotation rate (i.e., $\mathbf{G} \approx \Omega^2\,\mathbf{r}$) leads to the following simplifications: $f \to 0$ and $\cos\varphi \to 1$ as shown in Fig. 3(c). Consequently, the linear momentum equations Eq. (4) can be expressed by

$$\frac{\mathrm{D}u}{\mathrm{D}t} + 2\Omega w = -\frac{1}{\rho}\frac{\partial p}{\partial x},$$

$$\frac{\mathrm{D}v}{\mathrm{D}t} = -\frac{1}{\rho}\frac{\partial p}{\partial y}, \tag{6}$$

$$\frac{\mathrm{D}w}{\mathrm{D}t} - 2\Omega u = -\frac{1}{\rho}\frac{\partial p}{\partial z} + \Omega^2 z.$$

Note that the r-direction aligns with the z-direction in the reference frame of the rotating bucket. Evidently, this approximation is applied to the phenomena where the vertical motion w is important, and the Coriolis effect represents the state in the equatorial region, instead of the polar region.

It is remarked here that, to my knowledge, only a few centrifuge studies for geophysical hydrodynamics were found in the literature. Sheremet [15] studied the effects of both vertical and horizontal components of Earth's rotation on deep-water thermal convection plumes, using a centrifuge to swing a bucket by 30° at a very slow rotation rate. On the other hand, using a fast-rotating cylindrical annulus apparatus, Jiang et al. [16] reported a study on turbulent thermal convection in the high Rayleigh number regime.

Centrifuge experiments for equatorial currents

The equatorial region in the Pacific Ocean plays an important role in the global climate, which is affected by the El Niño-Southern Oscillation. While its dynamics in the atmosphere and ocean are closely interrelated, one factor of the mechanism is the Ekman transport of the ocean-surface layer driven by the stresses of easterly trade winds [17-20]. The resulting divergence of the surface layer toward north and south from the equatorial region induces upwelling along the equator as illustrated in Fig. 4: this phenomenon is called the Ekman suction. This upwelling raises the cold-water mass to the surface. This is a common explanation for La Niña. This mechanism is usually explained based on the "traditional approximation", ignoring the horizontal component of Earth's rotation, in spite of the fact that the horizontal component of Earth's rotation dominates in the equatorial region and the vertical component vanishes at the equator: i.e., $f \to 0$ and $\cos\varphi \to 1$.

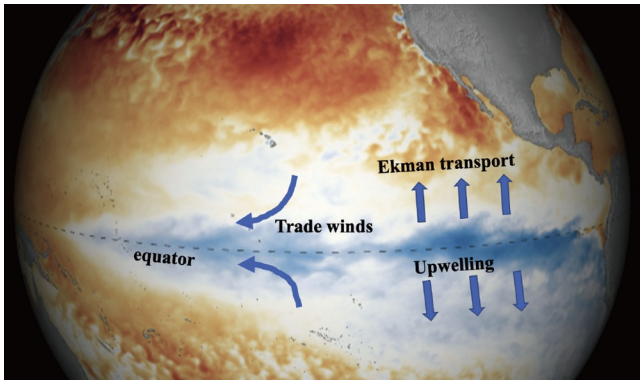

Figure 4 Sea surface temperature anomaly during the 2020 La Niña (based on Climate.gov/NNVL). The easterly trade-wind stress induces the Ekman transports toward north and south from the equatorial region, resulting in upwelling along the equator.

Studying the geophysical fluid dynamics where the Coriolis effect is important, we must attempt to match the Rossby number for the model and prototype: $R_b = u_0/(2\Omega L_0)$: see Eq. (2). Consider a scaled-down experiment in the centrifuge with $L_r = L_m/L_p$, and the centrifuge rotation $\Omega_r = \Omega_m/\Omega_p$. Then, to satisfy the Rossby number, the velocity scale must be $u_r = u_m/u_p = \Omega_r L_r$ and the time scale $T_r = t_m/t_p = 1/\Omega_r$. With Earth's rotation $\Omega_p = 7.292\times10^{-5}$ rad/s (1 revolution per day), the upper ocean of our interest is, say, $L_p \approx 100$ m, and the upwelling velocity $u_p \sim 3$ m/day (3.5×10^{-5} m/s) (see Ref. [21]), the Rossby number is approximately $R_b \sim O(10^{-3})$. Considering the existing centrifuge facility at the University of California, Davis, a realistic scale of the model installed in the centrifuge is $L_m = 0.5$ m and the rotation rate of the centrifuge is set at $\Omega_m = 4.4$ rad/s ($= 20g$). The resulting scaling factors for this model would be $L_r = 1/200$, $\Omega_r = 60000$, $u_r = 300$, and $t_r = 1/60000$. With this model scale, a fortnightly phenomenon in the ocean can be realized in approximately 20 s in the centrifuge model. Incidentally, matching the Rossby number, the Reynolds number mismatches slightly: in this case, $\Omega_r L_r^2 = 1.5$ (the model Reynolds number is 1.5 times that of the prototype).

It is anticipated that the Coriolis effect would tend to veer the upwelling flow caused by Ekman suction and would result in the formation of the clockwise circulation in the tank as illustrated in Fig. 3(c); I anticipate that the multiple circulation cells would be formed if the model were sufficiently long. This potential mechanism of Coriolis-induced circulation cells could play an important role in the upper-ocean mixing in the equatorial region during El Niña. This is a conjecture.

Other possibilities for the use of centrifuge would be the studies on internal waves in the equatorial currents and deep-water mixing on the sloping boundary. Similar studies can be considered for the topics of astrophysical fluid dynamics. For example, Fig. 5 shows an image of Jupiter, where the Coriolis effect must affect the flow pattern. The centrifuge can be used to explore such fluid dynamics, in particular for the region along the equator. It is emphasized that a centrifuge is the only apparatus capable of mimicking the Coriolis effect in the equatorial region where the hor-

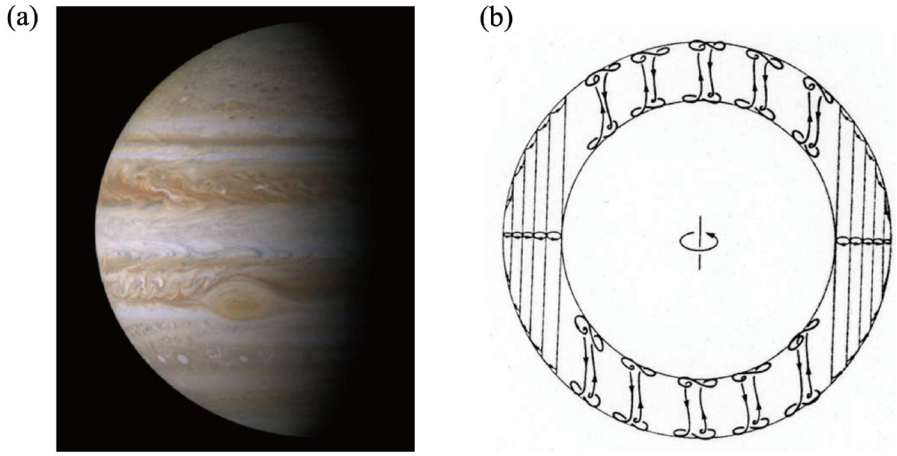

Figure 5 (a) A photo of Jupiter (radius ≈ 70000 km and rotation rate $\Omega = 1.75 \times 10^{-4}$/s (1 day ≈ 10 h)) and (b) a sketch of the convection pattern given by Busse [22].

izontal component of Earth's rotation effect dominates over the vertical component.

5. Summary

In this brief exposition, we first present the scaling law for fluid dynamics that is applied to a scaled-down model to achieve the dynamic similitudes. Because the continuum hypothesis is valid in fluid dynamics, the constitutive relation is well accepted. Consequently, the scaling law can be derived systematically by nondimensionalizing the governing equations and boundary conditions. The resulting scaling law is, however, theoretical. Under a normal circumstance, it is formidable to completely satisfy the scaling law because fluid properties (such as the fluid density, viscosity, and surface tension) and the body force (gravity) cannot be controlled in practice. However, producing a hypergravity field by centrifuge is a means to control the body force in the model, which can substantially reduce the scale effect.

Advantages of the hypergravity experiments:

(1) A larger Reynolds number in the small-scale model: once the Reynolds number is large enough, then the viscous effect becomes unimportant and precise matching in Reynolds number may not affect the flow characteristics and behaviors in the model.

(2) Because the model size is limited due to the space available in the bucket of the centrifuge, it is possible to use a fluid other than water to reduce the scale effect. For example, Exton [23] used a viscous fluid (a mixture of hydroxypropyl methylcellulose and water) to saturate the model sediments in the model. On the contrary, for experiments in hydrodynamics, we need to use a less viscous fluid for increasing the value of the Reynolds number in the model to mimic the prototype condition.

Disadvantages of the hypergravity experiments:

(1) The model must be designed and constructed to withstand the forces under the substantially enhanced body force.

(2) Because the model size must be small and the model time scale is fast, instruments used in the model must be sufficiently small, durable under the high stresses, and capable of capturing data at a high sampling rate with a high resolution.

(3) Because the centrifuge arm length is finite, fluid motions in the radial and azimuthal directions in the model be affected by the Coriolis effect.

While the Coriolis effect is undesirable in most centrifuge experiments, we, instead, utilize this effect for geophysical fluid dynamic simulations. The rotating table (Fig. 3(b)) is often used to investigate geophysical fluid dynamics under the traditional approximation (neglecting the horizontal component of rotation). On the other hand, the centrifuge creates the condition such that the horizontal component of the rotation is dominant and the vertical component is practically nil under the high-speed rotation. Consequently, the centrifuge is capable of mimicking the Coriolis effect in the equatorial region. Because the hypergravity field can reduce the scale effect by the enhancement of the Reynolds number as well as the Weber number and Bond number, we propose other potential usages of geotechnical centrifuge apparatuses to study a variety of hydrodynamics problems (e.g., bubble/droplet dynamics, density currents).

Conflict of interest *On behalf of all authors, the corresponding author states that there is no conflict of interest.*

Acknowledgements *The work was supported by the US National Science Foundation (Grant No. CMMI-1538211). Rick Fragaszy and Bruce Kutter initiated the discussions for seeking potential usages of geophysical centrifuge apparatuses.*

1 S. Sassa, and H. Sekiguchi, Analysis of wave-induced liquefaction of sand beds, Géotechnique **51**, 115 (2001).
2 M. Exton, S. Harry, H. B. Mason, H. Yeh, and B. Kutter, in Novel experimental devise to simulate tsunami loading in a geotechnical centrifuge: Proceedings of 9th International Conference Physical Modelling in Geotechnics 2018, London, 2018.
3 M. Exton, S. Harry, B. Kutter, H. B. Mason, and H. Yeh, Simulating tsunami inundation and soil response in a large centrifuge, Sci. Rep. **9**, 1 (2019).
4 M. Exton, and H. Yeh, Effects of an impermeable layer on pore pressure response to tsunami-like inundation, Proc. R. Soc. A **478**, 20210605 (2022).
5 S. Harry, M. Exton, and H. Yeh, Boulder pickup by tsunami surge, J. Earthquake Tsunami **13**, 1941006 (2019).
6 H. Takahashi, S. Sassa, Y. Morikawa, D. Takano, and K. Maruyama, Stability of caisson-type breakwater foundation under tsunami-induced seepage, Soils Found. **54**, 789 (2014).
7 S. Sassa, H. Takahashi, Y. Morikawa, and D. Takano, Effect of overflow and seepage coupling on tsunami-induced instability of caisson breakwaters, Coast. Eng. **117**, 157 (2016).
8 K. Ueda, S. Iai, and T. Tobita, Centrifuge model tests and large deformation analyses of a breakwater subject to combined effects of tsunami, Soil Dyn. Earthquake Eng. **91**, 294 (2016).
9 H. Yeh, Free-surface dynamics, in: Advances in Coastal and Ocean Engineering, edited by P. L.-F. Liu (World Scientific Publishing Co., Singapore, 1994), pp. 1-75.
10 S. L. Lingel, Scaling Effects on the Mixing Processes of Lock-Exchange Gravity Currents, Dissertation for Doctoral Degree (University of Washington, Seattle, 1997).
11 S. A. Thorpe, Turbulence and mixing in a Scottish Loch, Phil. Trans. Royal Soc. London **A286**, 125 (1977).
12 T. M. Dillon, The energetics of overturning structures: Implications for the theory of fossil turbulence, J. Phys. Oceanogr. **14**, 541 (1984).
13 P. S. Galbraith, and D. E. Kelley, Identifying overturns in CTD profiles, J. Atmos. Ocean. Technol. **13**, 688 (1996).
14 P. E. Dimotakis, The mixing transition in turbulent flows, J. Fluid Mech. **409**, 69 (2000).
15 V. A. Sheremet, Laboratory experiments with tilted convective plumes on a centrifuge: a finite angle between the buoyancy force and the axis of rotation, J. Fluid Mech. **506**, 217 (2004).
16 H. Jiang, X. Zhu, D. Wang, S. G. Huisman, and C. Sun, Super-gravitational turbulent thermal convection, Sci. Adv. **6**, eabb8676 (2020).
17 A. E. Gill, Atmosphere—Ocean Dynamics (Elsevier, 2016).
18 E. B. Kraus, and S. Levitus, Annual heat flux variations across the tropic circles, J. Phys. Oceanogr. **16**, 1479 (1986).
19 M. A. Alexander, and J. D. Scott, The role of ekman ocean heat transport in the northern hemisphere response to ENSO, J. Clim. **21**, 5688 (2008).
20 R. H. Weisberg, and L. Qiao, Equatorial upwelling in the central pacific estimated from moored velocity profilers, J. Phys. Oceanogr. **30**, 105 (2000).
21 M. E. Carr, Simulation of carbon pathways in the planktonic ecosystem off Peru during the 1997-1998 El Niño and La Niña, J. Geophys. Res. **108**, 3380 (2003).
22 F. H. Busse, Convection driven zonal flows and vortices in the major planets, Chaos-An Interdisciplinary J. Nonlinear Sci. **4**, 123 (1994).
23 Exton, Centrifuge Modeling of Soil Response to Tsunami-like Rapid Flooding and the Subsequent Drawdown, Dissertation for Doctoral Degree (Oregon State University, Cornwallis, 2019).

超重力场中的地球流体动力学

Harry Yeh

摘要 超重力可以通过在离心机装置中创建由向心加速度施加的场来实现. 这样的装置通常用于测试岩土工程问题中的土壤响应. 本文介绍了离心机装置在研究流体力学中各种主题的潜在应用. 本文首先回顾了与流体力学相关的尺度定律, 并描述了控制体积力的优势. 在这样的实验中, 其中一个被认为是不利因素的是离心机中存在的科里奥利效应. 然而, 我们提出利用这种效应来研究在赤道地区特别发生的地球物理流体动力学问题, 从而将其转化为我们的优势.